Advanced extreme ultraviolet resist testing using the SEMATECH Berkeley 0.3-NA microfield exposure tool

Patrick P. Naulleau,[1] Christopher N. Anderson,[2] Jerrin Chiu,[1] Kim Dean,[3] Paul Denham,[1] Kenneth A. Goldberg,[1] Brian Hoef,[1] Sungmin Huh, [4] Gideon Jones,[1] Bruno La Fontaine,[5] Andy Ma,[6] Dimitra Niakoula,[1]Joo-on Park,[6] and Tom Wallow[5]

[1]Center for X-Ray Optics, Lawrence Berkeley National Laboratory, Berkeley, CA 94720
[2]Applied Science & Technology Dept., University of California, Berkeley, CA 94720
[3]SEMATECH, Austin, TX 78741
[4]Samsung Electronics, Korea
[5]Advanced Micro Devices, Sunnyvale, CA 94088
[6]SEMATECH, Albany, NY 12203

ABSTRACT

Microfield exposure tools (METs) continue to play a dominant role in the development of extreme ultraviolet (EUV) resists. Here we present an update on the SEMATECH Berkeley 0.3-NA MET and summarize the latest test results from high-resolution line-space and contact-hole printing. In practice, the resolution limit of contact-hole printing is generally dominated by contact size variation that is often speculated to originate form shot noise effects. Such observations of photon-noise limited performance are concerning because they suggest that future increased resist sensitivity would not be feasible. Recent printing data, however, indicates that the contact size variation problem is currently not a result of shot noise but rather attributable to the mask in combination with the resist-dominated mask error enhancement factor (MEEF). Also discussed is the importance of the contribution of the system-level line-edge roughness (LER) to resist LER values currently obtained with the SEMATECH Berkeley MET. We present the expected magnitude of such effects and compare the results to observed trends in LER performance from EUV resists over the past few years.

Keywords: extreme ultraviolet, lithography, photoresist, aberrations

1. INTRODUCTION

As extreme ultraviolet (EUV) lithography approaches commercialization, resist issues remain an important challenge. In particular, simultaneously meeting resolution, line-edge roughness (LER), and sensitivity specifications is the primary issue resist developers face. Excellent progress has been made in the crucial area of resolution, however, LER and sensitivity still need improvement. Because photospeed has direct impact on ultimate EUV source power requirements and the source is widely believed to be the most daunting challenge facing EUV commercialization, resist sensitivity is particularly important for EUV. Moreover, photospeed is also tightly linked to LER noting that, in general, observations show that faster resists suffer from larger LER.

Microfield exposure tools (METs) [1-3] play a particularly important role in the area of resist development. This is due to the fact that the relative simplicity of such tools, in general, enables them to provide higher resolution capabilities than production scale alpha tools. For example, preproduction/alpha tools just now being developed/delivered [4,5] have numerical apertures (NA) of 0.25 as compared to the 0.3-NA available from the latest EUV METs.

Here we report on recent results from the SEMATECH Berkeley MET [1,6,7] operating as an EUV resist and mask test center since early 2004. The SEMATECH Berkeley exposure tool utilizes a 5×-reduction, 0.3-NA optic [8,9] fabricated by Zeiss and has a well-corrected field of view of 1×3 mm at the reticle plane (200×600 μm at the wafer plane). The CAD model shown in Fig. 1 depicts the major components of the exposure station as well as the EUV beam path (the system is described in detail in Ref. 1). With a NA of 0.3, the MET optic has a resolution of 22.5 nm at a k_1 factor of 0.5 and a resolution of 16-nm at a k_1 factor of 0.35.

Emerging Lithographic Technologies XII, edited by Frank M. Schellenberg
Proc. of SPIE Vol. 6921, 69213N, (2008) · 0277-786X/08/$18 · doi: 10.1117/12.773833

Although the SEMATECH Berkeley MET utilizes essentially the same projection optics design as commercial METs [2,3], the unique lossless programmable coherence illuminator [10] of the Berkeley tool allows it to achieve considerably lower k_1 factors (thus better resolution) than other tools.

2. TOOL PERFORMANCE

Another significant benefit of the SEMATECH Berkeley MET is that it is the only MET to have been interferometrically aligned at EUV wavelengths after integration into the final tool body at the operational location thereby ensuring optimal performance [11]. Since the original interferometric alignment, we have monitored wavefront stability using lithographic measurements of low-order aberrations including astigmatism and spherical error [12,13]. Here we report on a full field measurement of the astigmatism performed one year after our last astigmatism measurement and four years after the final interferometric alignment of the optic.

As previously described, we characterize the astigmatism (magnitude and direction) by measuring the relative longitudinal focal positions of four orthogonal feature orientations [14]. In particular, we use orientations of 0° (horizontal), 90° (vertical), -45°, and 45°. Figure 2 shows an example of the 45-nm half-pitch pattern we use. This pattern is replicated at 9 points across the field in a two-dimensional grid in order to characterize the field dependence of the aberrations.

Figure 3 shows the recently measured astigmatism along with lithographic values reported two years ago [12]. Noting that the uncertainty in each measurement is approximately 0.1-nm rms, the vast majority of the values appear unchanged. In cases where arguably there are statistically relevant changes, the majority represent reductions in measured astigmatism compared to two years ago. The current field averaged astigmatism value is 0.34-nm rms and the value from two years ago was 0.42-nm rms. It is also interesting to note that these results were obtained despite the occurrence of a substantial earthquake affecting the exposure tool during the period between the two measurements. The shaking was severe enough to break shear bolts on an MET stage, however, the results show no detrimental results to the optic.

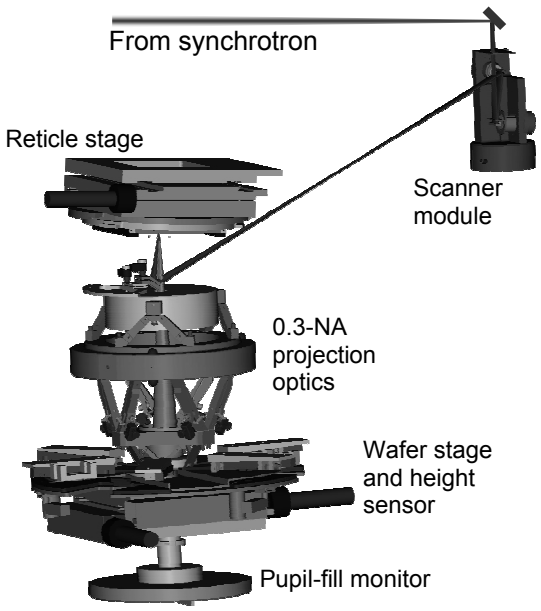

Fig. 1. CAD model of the Berkeley MET exposure tool.

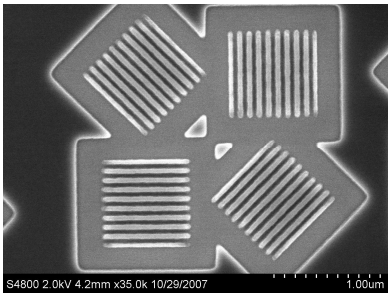

Fig. 2. Printed 45-nm half-pitch quad orthogonal orientation pattern used to characterize astigmatism. This image was recorded in the top right corner of the field.

In addition to extracting astigmatism information, the same source data can be used to determine average field curvature. In this case we take the nominal focus at each location in the field to be the average focus of all four orientations. Figure 4 shows the raw measured field curvature as well as the tilt corrected result in nm of focus shift. The field is found to have approximately 25-nm of tilt oriented along the short direction of the field. With tilt removed, the peak-to-valley focus variation is 25 nm and the rms variation is 8 nm. We note that the rms field error is essentially identical in magnitude to the lithographic focus measurement uncertainty previously reported for the focus determination method used here [14].

Another important quality metric for EUV optics is flare. Flare at EUV is fundamentally caused by high-frequency roughness on the projection optics leading to scatter. This scatter serves to add a low-level background to the image, thereby reducing the aerial-image contrast. EUV optics are particularly vulnerable to this problem owing to the short

wavelength used. As previously reported [15], the flare in the SEMATECH Berkeley MET was lithographically measured to be approximately 6% in a 1 μm line and consistent with predictions based on surface roughness characterization of the MET optics. Figure 5 shows results from a recent re-characterization of the flare demonstrating that the flare has remained statistically unchanged over the 3.5 years since the last reported measurement was made.

5/2005

0° astigmatism (rms nm)

-0.5	-0.4	-0.2
-0.5	-0.4	0.0
-0.5	-0.5	0.0

45° astigmatism (rms nm)

0.0	-0.2	-0.3
0.0	-0.1	-0.2
0.0	-0.1	-0.2

Total astigmatism magnitude (rms nm)

0.5	0.5	0.4
0.5	0.4	0.2
0.5	0.6	0.2

10/2007

0° astigmatism (rms nm)

-0.5	-0.3	-0.2
-0.5	-0.5	-0.2
-0.2	-0.3	-0.1

45° astigmatism (rms nm)

-0.1	0.0	0.0
0.0	-0.1	-0.1
0.0	0.0	-0.2

Total astigmatism magnitude (rms nm)

0.5	0.3	0.2
0.5	0.5	0.3
0.2	0.3	0.3

Fig. 3. Lithographically measured astigmatism across the field. Reported results are rms magnitudes in nm. The locations in the table correspond to the physical locations of the measured site in the field. For comparison, we include results from two years ago [12].

Field curvature raw (nm)

8	31	5
-3	-6	0
-9	-6	-19

Field curvature tilt removed (nm)

-7	18	-7
-5	-6	2
2	7	-4

Fig. 4. Lithographically measured field curvature in nm.

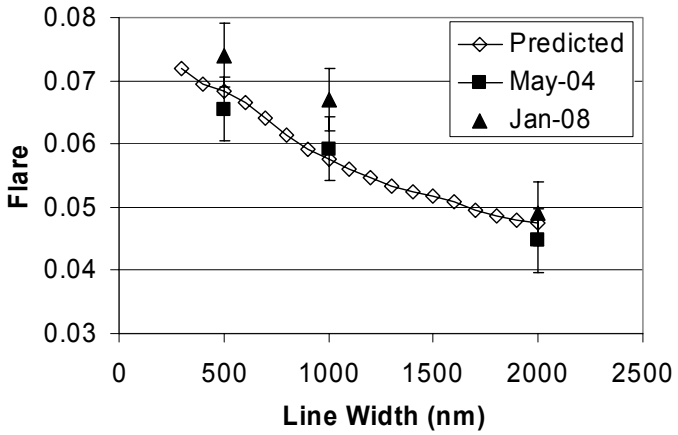

Fig. 5. Lithographic flare measured in the SEMATECH Berkeley MET from Jan. 2008 compared to measured values from 2004 and predicted values. No statistically relevant changes seen in past 3.5 years.

In addition to projection optics metrics, we also track system performance metrics such as focus control as determined from wafer-to-wafer focus variation. Many factors contribute to focus variations including wafer flatness, coating quality, and coating characteristics such as thickness and optical properties. In the values reported we try to null-out the effects of coating thickness by comparing the wafer-to-wafer focus change for similar resist parameters only. We note that concentrating on wafer-to-wafer focus reproducibility also has the effect of nulling out long timescale focus drifts in the tool.

Figure 6 shows the focus stability results for tracking data over the past two years. The square symbols represent data before a focus sensor upgrade performed in March 2007. Prior to the upgrade the wafer-to-wafer focus stability was 91-nm rms. The focus upgrade was comprised of significantly increasing the speed of the wafer-height sensor electronics thereby allowing it to be directly used as the piezo-actuation feedback bypassing the integrated piezo-stack strain gauges. Following the upgrade, wafer-to-wafer-focus control was improved to 44-nm rms. Note the 44-nm value includes the triangular points in Fig. 6 which we actually consider as well-explained outliers. The two overlapping points at 200-nm focus shift were a result of a communications interface timing error which caused a DC shift of the focus value. The problem was identified after two wafers and corrected. The later two overlapping points at 150-nm focus shift can be attributed to a temperature change caused by illuminator preventative maintenance carried out the day prior to the exposures. As the temperature stabilized throughout the day, the focus returned to normal operating range. Another significant benefit of the recent focus system upgrade is improved intra-wafer focus control. The intra-wafer focus control stability was improved from 21.4-nm rms to 1.8-nm rms.

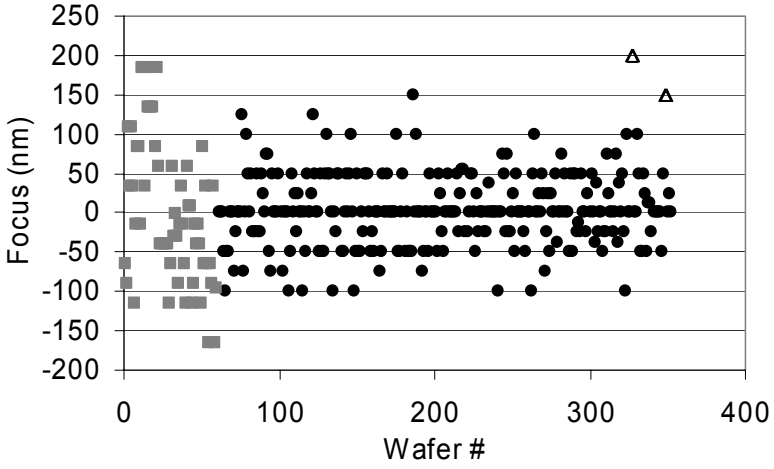

Fig. 6. Wafer-to-wafer focus stability over the past two years. Square gray points represent data prior to recent upgrade with a stability of 91 nm rms. Circle black points represent data after the upgrade with a stability of 44 nm rms.

Finally we consider system uptime. In 2007 the system was down for only approximately 4.5 shifts out of the scheduled 187 shifts (~98% uptime). Two of those lost shifts were due to the earthquake event mentioned above and the remainder of the lost shifts were due to issues with the synchrotron itself. We note that the majority of the lost time was recovered through agreements with other users of the undulator beamline supporting the MET bringing the effective uptime to nearly 100%.

3. MASK-INDUCED LER

As resist performance pushes to ever smaller line-edge roughness (LER) levels, the question of system-level contributors becomes increasingly important. Examples of such system-level effects include LER on the mask itself [16] and mask reflector surface roughness [17,18]. Here we examine the importance of these effects in the SEMATECH Berkeley MET and consider their contribution to the recently observed ~2.5-nm LER performance floor. Aerial image modeling is performed using measured values for mask LER and mask multilayer roughness for the most recent MET mask. The modeling further includes the effects of the well-characterized MET flare, wavefront, and pupil characteristics [19-22].

Figure 7 shows the aerial-image LER computed on 50-nm lines and spaces for four different illumination settings. We see that the higher coherence settings (monopole and dipole) have the largest best-focus LER values. This is consistent with the aerial-image LER being dominated by mask multilayer roughness. Note that the computed aerial-image LER values are quite close to recently observed resist LER limits. To quantify the relative importance of the mask LER, we assume the mask contributors to add in quadrature with other LER terms. Figure 8(a) shows a scatter plot of the directly observed resist LER over the past few years as a function of sensitivity; the vast majority of this data was recorded under annular illumination. Figure 8(b) shows the same data after quadrature subtraction of the mask LER assuming the lowest modeled LER value of 1.43 nm for annular 0.35-0.55 illumination from Fig. 7. The results show that despite apparent significant mask contributions, resist LER remains the dominant factor.

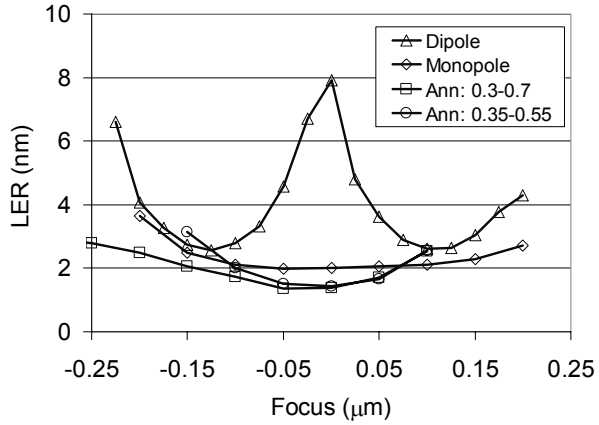

Fig. 7. Predicted aerial-image LER for the SEMATECH Berkeley MET under various illumination conditions.

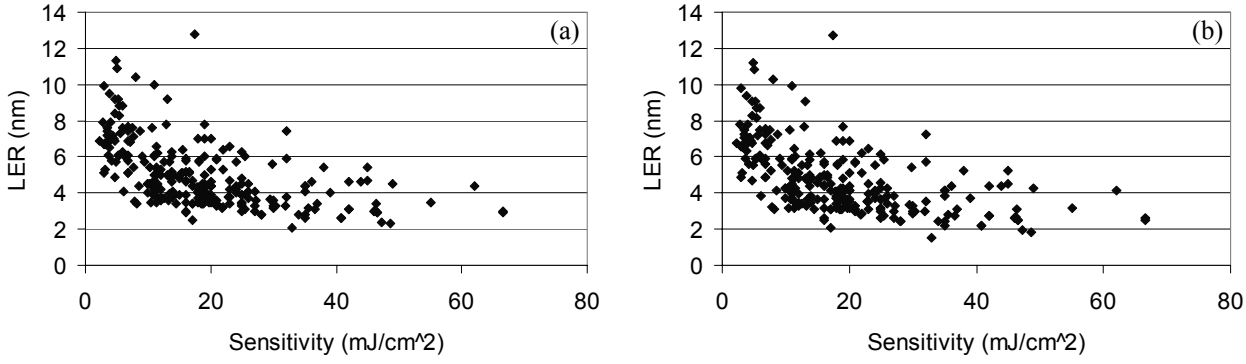

Fig. 8. (a) Scatter plot of directly observed resist LER over the past few years as a function of sensitivity and (b) same data "corrected" by removing the aerial-image contribution to the LER. The best focus annular LER value of 1.43 nm is used. The results show that despite apparent significant mask contributions, resist LER remains the dominant factor.

3. CONTACT-SIZE VARIATION AND RESIST MEEF

One significant benefit of EUV over immersion 193-nm lithography is in the printing of contacts. This is due to the relatively large k_1 factor and resulting small mask error enhancement factor (MEEF). Figure 9 shows the computed aerial-image MEEF for 35-nm 1:2 contacts for the SEMATECH Berkeley MET. In this simulation a 2.8-nm symmetric shrink error is added to one of the contacts on the mask. The modeling shows the aerial-image MEEF to be 1 (i.e. no MEEF).

Despite the negligible MEEF, significant printed contact size variations are routinely observed. Figure 10 shows printed 35-nm 1:2 contacts in a 80-nm thick layer of chemically amplified Rohm and Haas resist with a dose to clear of approximately 10 mJ/cm^2. At first one might expect this variation to arise simply from shot noise, however, inspection of the various exposures in Fig. 10, for example, demonstrates that the relative sizes of the contacts are reproducible across various exposures, suggesting that the error actually originates from the mask.

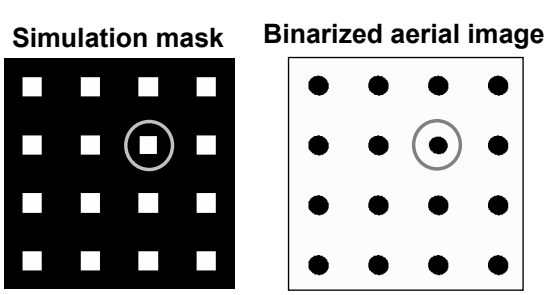

Fig. 9. Simulation of aerial image mask error enhancement factor for 35-nm 1:2 contacts in the SEMATECH Berkeley MET. Results show the MEEF to be unity.

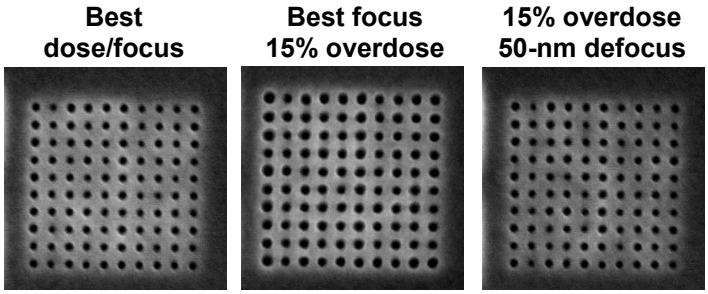

Fig. 10. Contact holes printed in a 80-nm thick layer of Rohm and Haas resist using the Berkeley MET tool with a conventional binary mask and conventional annular illumination ($0.35 < \sigma < 0.55$).

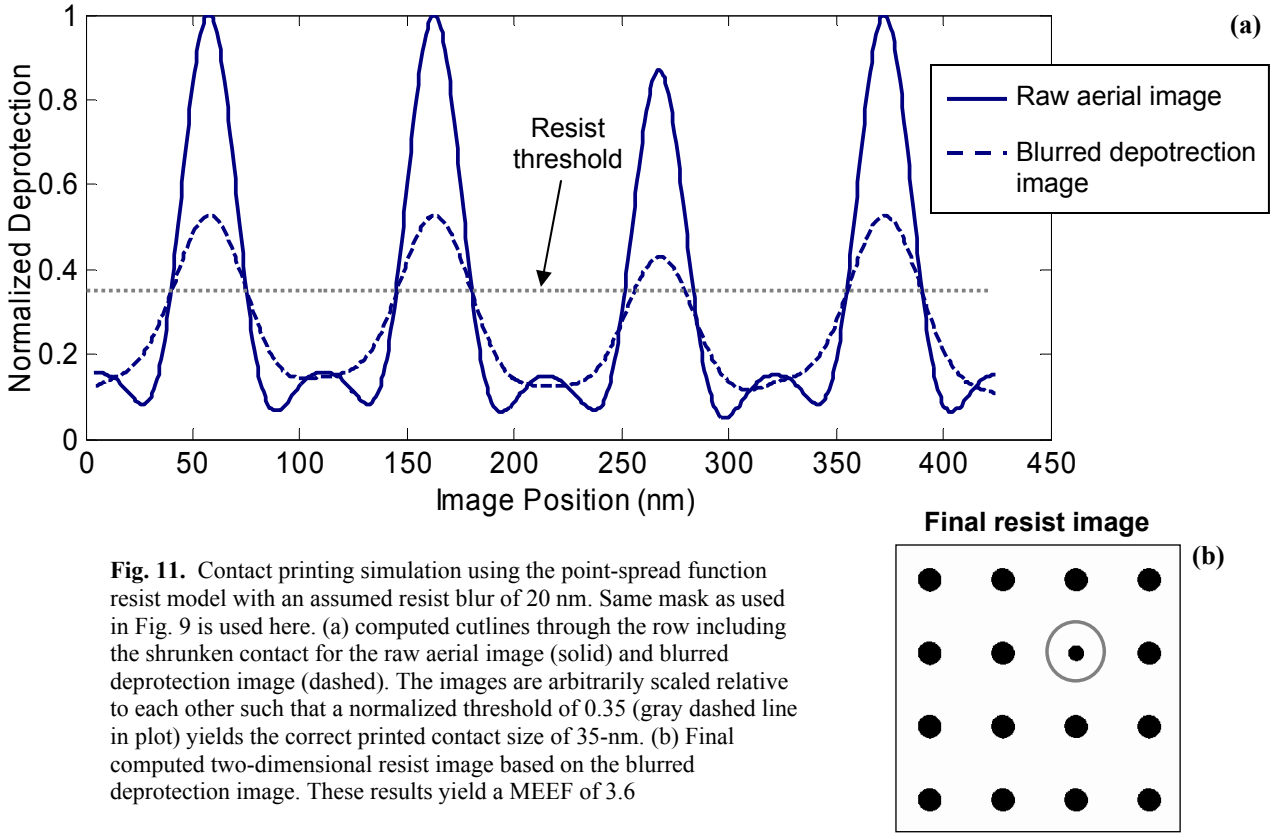

Fig. 11. Contact printing simulation using the point-spread function resist model with an assumed resist blur of 20 nm. Same mask as used in Fig. 9 is used here. (a) computed cutlines through the row including the shrunken contact for the raw aerial image (solid) and blurred deprotection image (dashed). The images are arbitrarily scaled relative to each other such that a normalized threshold of 0.35 (gray dashed line in plot) yields the correct printed contact size of 35-nm. (b) Final computed two-dimensional resist image based on the blurred deprotection image. These results yield a MEEF of 3.6

Analysis of the printed contact sizes in Fig. 10 shows the rms variation to be 3.2 nm. Similar analysis on the mask, however, shows a variation in wafer coordinates of only 1.1 nm. Using the unity MEEF value presented above, it is evident that mask errors alone cannot explain the observed printed contact size variation. As previously demonstrated [23], however, EUV system resolution limits are dominated by the resist not the aerial-image. It stands to reason then that the resist rather than the aerial image would play the dominant role in the MEEF. Treating resist effects as a point-spread function [24-26], we repeat the simulation from Fig. 9 with 20-nm of resist blur. Figure 11(a) shows the computed cutlines through the row including the shrunken contact for the raw aerial image (solid) and blurred deprotection image (dashed). The images are arbitrarily scaled relative to each other such that a normalized threshold of 0.35 (gray dashed line in plot) yields the correct printed contact size of 35-nm. The results show the enhancing effect of the resist blur on the MEEF. Figure 11(b) shows the final computed two-dimensional resist image based on the blurred deprotection image again demonstrating the resist-enhanced MEEF. These results yield a MEEF of 3.6 which when combined with the measured mask error results is consistent with observed contact size variation in resist.

4. RECENT RESIST TESTING RESULTS

Impressive resist performance improvements have been made both for line space and contact printing over the past year. We begin by considering line space printing. Figure 12 shows results from a resist with a dose to size of ~40 mJ/cm^2. Low-LER line/space printing is shown down to 32 nm. The LER values for 40 nm and 36 nm lines, respectively, are 2.5 nm and 2.8 nm. Moreover, Fig. 13 shows process window results for 40 nm and 36 nm half-pitch lines with annular illumination.

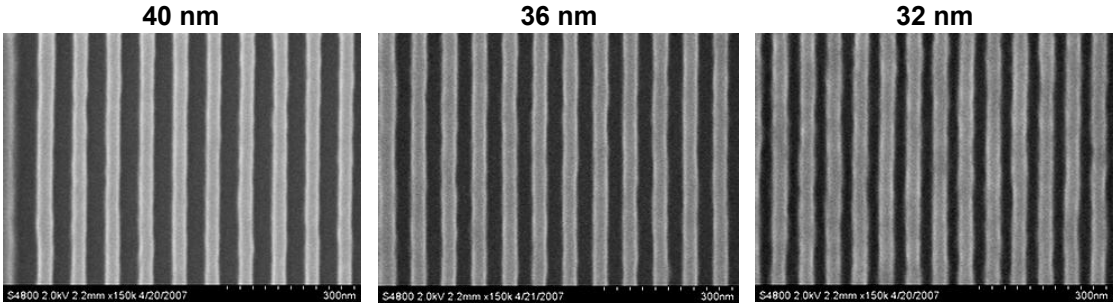

Fig. 12. Line space printing at low LER in a resist with dose to size of ~40 mJ/cm^2. The LER values for 40 nm and 36 nm lines, respectively, are 2.5 nm and 2.8 nm. Resist thickness is 80 nm.

As resist formulations improve, resist development efforts are including increasing amounts of process studies. Figure 14 shows PAB/PEB bake temperature study results in a ~20mJ/cm^2 resist. The results show 26-nm half-pitch lines exposed with rotated dipole illumination. Under the best conditions, an LER of 2.8-nm is achieved. More details on these tests can be found in Ref. [27].

Next we present recently achieved results demonstrating reasonable printing down to the 22-nm half-pitch level. Figure 15 shows rotated dipole printing results in another ~20mJ/cm^2 resist. Very impressive performance is observed down to the 24-nm half pitch level, at 22-nm we observe the initial onset of pattern collapse. We note that these results were obtained as part of SEMATECH's ongoing resist benchmarking program.

Finally we present contact hole printing results in two leading resists. Figure 16 shows 1:1 and 1:1.5 pitch contacts in a resist with a dose to clear of ~20 mJ/cm^2. The illumination setting was annular 0.35-0.55. Excellent 1:1 performance down to 35-nm is observed. Moreover, the resolution is readily pushed to 30 nm for the 1:1.5 pitch case. Figure 17 shows 1:1 contacts printed in a 80-nm thick layer of TOK EUVR-P1085 resist again using annular 0.35-0.55 illumination. Nice performance down to the 35-nm level is observed. Dose to clear in this resist is ~10 mJ/cm^2.

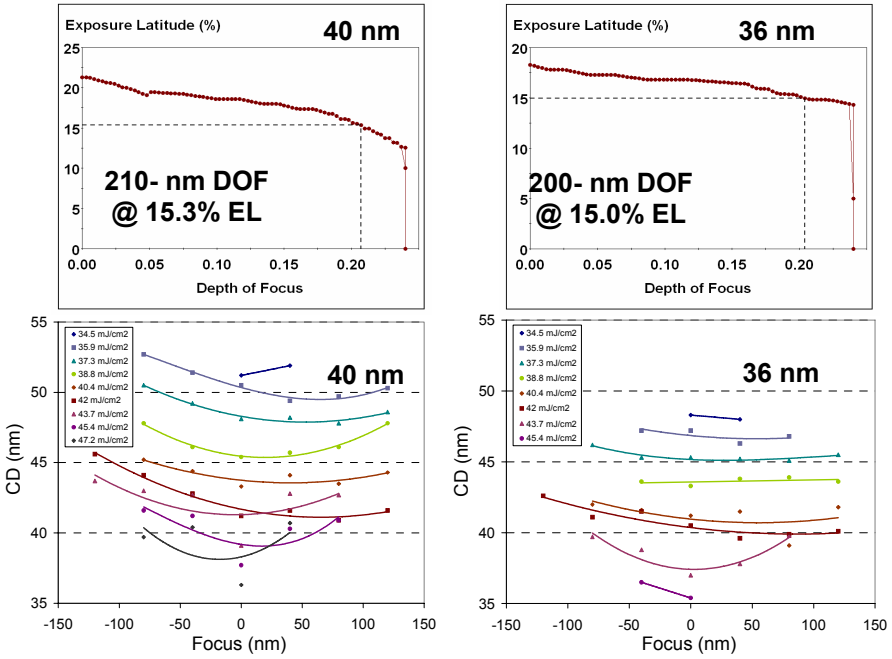

Fig. 13. Process window analysis results under annular illumination for the resist shown in Fig. 12.

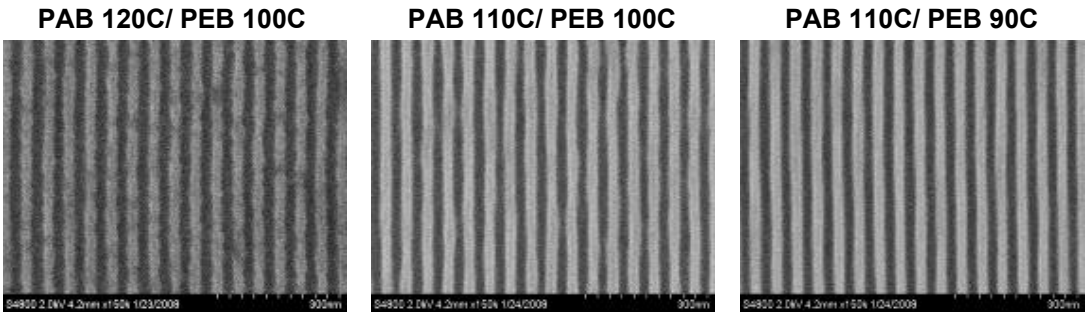

Fig. 14. PAB/PEB bake temperature study on 26-nm half-pitch lines exposed with rotated dipole illumination. Under the best conditions (PAB 110 C/ PEB 90 C), an LER of 2.8-nm is achieved. Resist thickness is 50 nm.

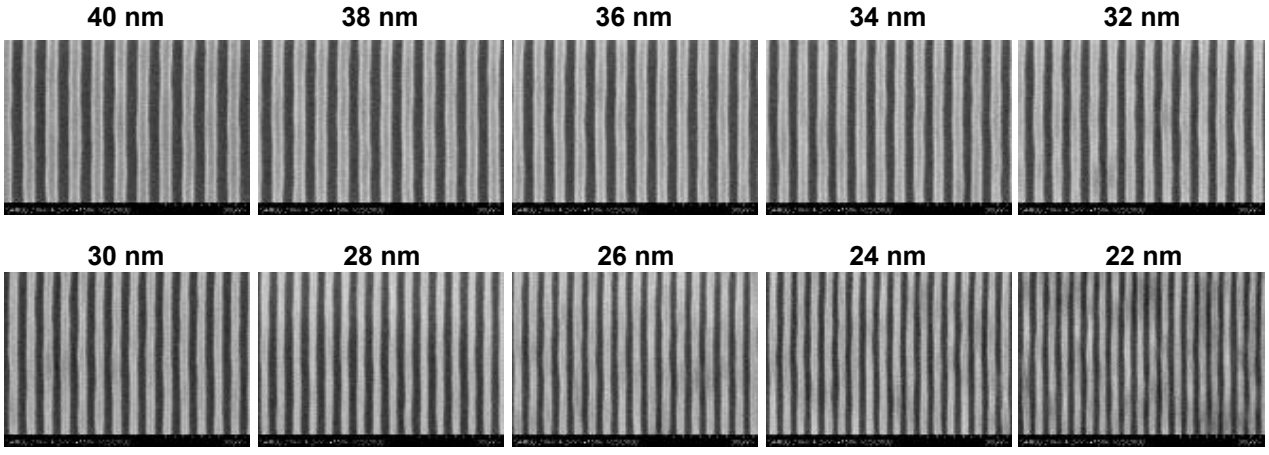

Fig. 15. Rotated dipole printing results as a function of pitch in a ~20mJ/cm^2 resist. Printing down to 22-nm demonstrated. Resist thickness is 50 nm.

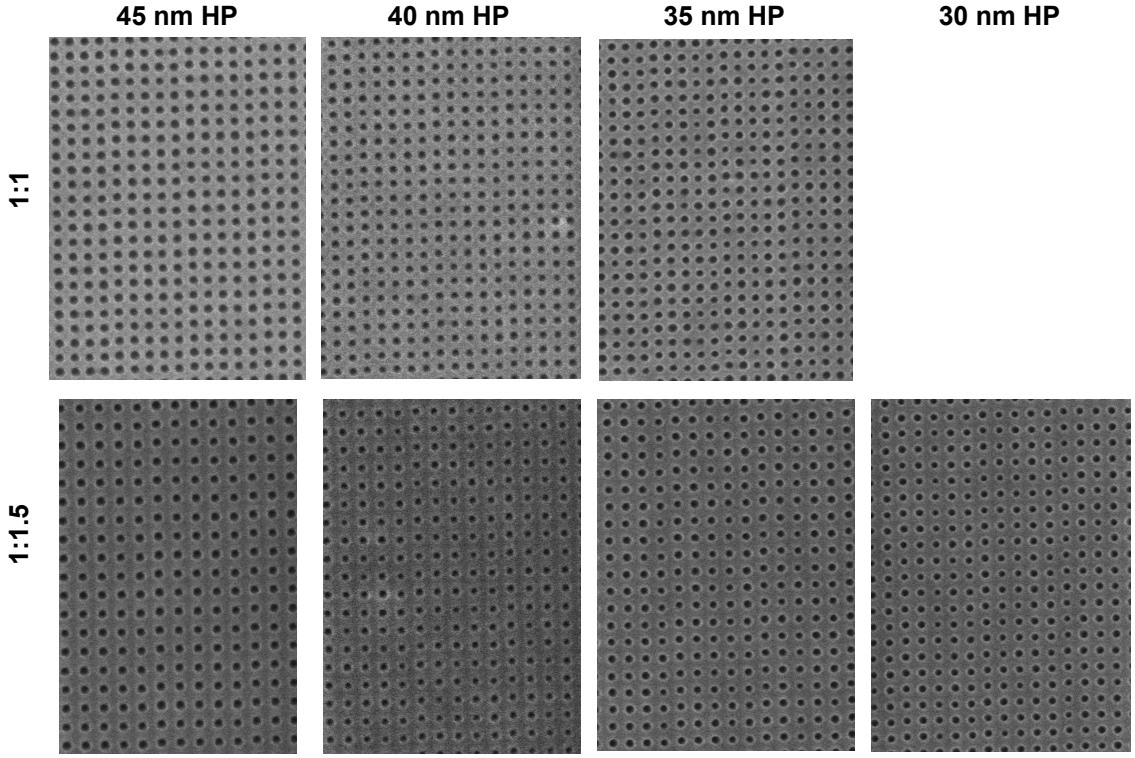

Fig. 16. 1:1 and 1:1.5 pitch contacts in a resist with a dose to clear of ~20 mJ/cm^2. The illumination setting was annular 0.35-0.55.

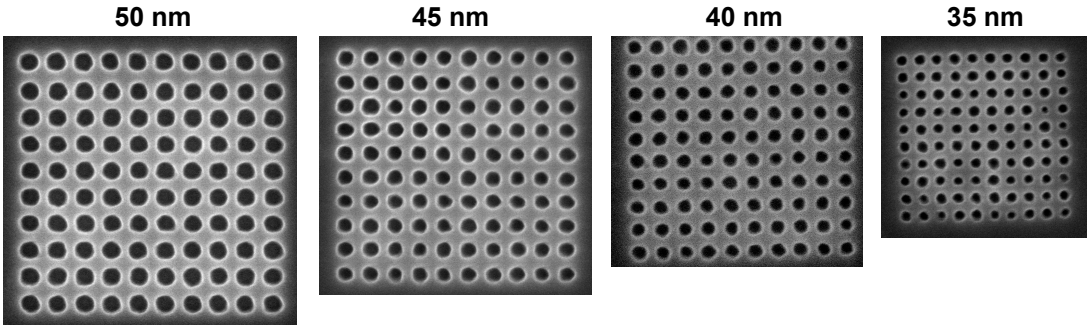

Fig. 17. 1:1 contacts printed in a 80-nm thick layer of TOK EUVR-P1085 resist again using annular 0.35-0.55 illumination.

5. SUMMARY

The SEMATECH Berkeley EUV microfield exposure tool continues to play a crucial role in the advancement of EUV. The unique programmable coherence properties of this tool enable it to achieve higher resolution than other 0.3-NA EUV tools. Over the past year the tool has been used to demonstrate resist resolution of 22 half pitch at an exposure dose of ~20 mJ/cm^2. Moreover, contact-hole resolution down to 30 nm has been shown. Also, contact size variation analysis in conjunction with modeling has been used to demonstrate the importance of resist MEEF in observed contact size non-uniformities. The importance of mask contributors to LER was also studied with the conclusion that the effects should indeed be considered, however, they cannot fully explain the experimentally observed lower LER bound.

With respect to tool performance, the long term aberration stability of the tool has again been verified through lithographic measurement of astigmatism across the entire field. Moreover, new flare measurements have revealed no statistically relevant flare changes in the past 3.5 years. Finally, focus system upgrades have improved the wafer-to-wafer rms focus stability from 91 nm to 44 nm and the intrawafer focus stability from 21.4 nm to 1.8 nm.

The authors are greatly indebted to the CXRO precision engineering team including Seno Rekawa, Kevin Bradley, Rene Delano, Drew Kemp, Jeff Gamsby, Bob Gunion, Ron Oort, Farhad Salmassi, and Ron Tackaberry for contributions in building and maintaining the tool. Moreover we thank Jim Thackeray of Rohm and Haas and Dave White and Koki Tamura of TOK for excellent resist support. This work was funded by SEMATECH and performed at Lawrence Berkeley National Laboratory using the SEMATECH MET exposure facility at the Advanced Light Source. Lawrence Berkeley National Laboratory's Advanced Light Source synchrotron facility is supported by the DOE, Office of Science, Basic Energy Sciences.

REFERENCES

1. P. Naulleau, *et al.*, "Status of EUV micro-exposure capabilities at the ALS using the 0.3-NA MET optic," Proc. SPIE **5374**, 881-891 (2004).
2. A. Brunton, *et al*., "High-resolution EUV imaging tools for resist exposure and aerial image monitoring," Proc. SPIE **5751**, 78-89 (2005).
3. H. Oizumi, Y. Tanaka, I. Nishiyama, H. Kondo, K. Murakami, "Lithographic performance of high-numerical-aperture (NA=0.3) EUV small-field exposure tool (HINA)," Proc. SPIE **5751**, 102-109 (2005).
4. H. Meiling, *et al*., "First performance results of the ASML alpha demo tool," Proc. SPIE **6151**, 615108 (2006).
5. M. Miura, K. Murakami, K. Suzuki, Y. Kohama, Y. Ohkubo, T. Asami, "Nikon EUVL development progress summary," Proc. SPIE **6151**, 615105 (2006).
6. P. Naulleau, K. Goldberg, E. Anderson, K. Dean, P. Denham, J. Cain, B. Hoef, K. Jackson, "Characterization of the synchrotron-based 0.3 numerical aperture extreme ultraviolet microexposure tool at the Advanced Light Source," J. Vac. Sci. & Technol. B **23**, 2840-2843 (2005).
7. J. Cain, P. Naulleau, C. Spanos, "Resist-based measurement of the contrast transfer function in a 0.3-numerical aperture extreme ultraviolet microfield optic," J. Vac. Sci. & Technol. B **24**, 326-330 (2006).
8. J. Taylor, D. Sweeney, R. Hudyma, L. Hale, T. Decker, G. Kubiak, W. Sweatt, N. Wester, "EUV Microexposure Tool (MET) for near-term development using a high NA projection system," 2nd International EUVL Workshop October 19-20, 2000, proceedings available from SEMATECH, Austin, TX.
9. R. Hudyma, J. Taylor, D. Sweeney, L. Hale, W. Sweatt, N. Wester, "E-D characteristics and aberration sensitivity of the Microexposure Tool (MET)," 2nd International EUVL Workshop October 19-20, 2000, proceedings available from SEMATECH, Austin, TX.
10. P. Naulleau, K. Goldberg, P. Batson, J. Bokor, P. Denham, and S. Rekawa, "A Fourier-synthesis custom-coherence illuminator for EUV microfield lithography," Appl. Opt. **42**, 820-826 (2003).
11. K. Goldberg, P. Naulleau, P. Denham, S. Rekawa, K. Jackson, E. Anderson, J. Liddle, "EUV interferometric testing and alignment of the 0.3 NA MET optic," Proc. SPIE **5374**, 64-73 (2004).
12. P. Naulleau, J. Cain, K. Dean, and K. Goldberg, "Lithographic Characterization of Low-Order Aberrations in a 0.3-NA EUV Microfield Exposure Tool," Proc. SPIE **6151**, 6151104 (2006).
13. P. Naulleau, C. Anderson, K. Dean, P. Denham, K. Goldberg, B. Hoef, B. La Fontaine, T. Wallow, "Recent results from the Berkeley 0.3-NA EUV microfield exposure tool," Proc SPIE **6517**, 65170V (2007).
14. P. Naulleau, J. Cain, K. Goldberg, "Lithographic characterization of the field dependent astigmatism and alignment stability of a 0.3 numerical aperture EUV microfield optic," J. Vac. Sci. & Technol. B **23**, 2003-2006 (2005).

15. J. Cain, P. Naulleau, E. Gullikson, C. Spanos, "Lithographic characterization of the flare in the Berkeley 0.3-numerical aperture extreme ultraviolet microfield optic," J. Vac. Sci. & Technol. B **24**, 1234-1237 (2006).
16. P. Naulleau and G. Gallatin, "The line-edge roughness transfer function and its application to determining mask effects in EUV resist characterization," Appl. Opt. **42**, 3390-3397 (2003).
17. N. Beaudry, T. Milster, "Effects of mask roughness and condenser scattering in EUVL systems," Proc. SPIE. **3676**, 653-662 (1999).
18. P. Naulleau, "The relevance of mask-roughness-induced printed line-edge roughness in recent and future EUV lithography tests," Appl. Opt. **43**, 4025-4032 (2004).
19. J. Cain, P. Naulleau, E. Gullikson, C. Spanos, "Lithographic characterization of the flare in the Berkeley 0.3-numerical aperture extreme ultraviolet microfield optic," J. Vac. Sci. & Technol. B **24**, 1234-1237 (2006).
20. K. Goldberg, P. Naulleau, P. Denham, S. Rekawa, K. Jackson, E. Anderson and J. Liddle, "At-Wavelength Alignment and Testing of the 0.3 NA MET Optic," J. Vac. Sci. & Technol. B **22**, 2956-2961 (2004).
21. P. Naulleau, J. Cain, K. Goldberg, "Lithographic characterization of the spherical error in an EUV optic using a programmable pupil fill illuminator," Appl. Opt. **45**, 1957-1963 (2006).
22. P. Naulleau, J. Cain, K. Goldberg, "Lithographic characterization of the field dependent astigmatism and alignment stability of a 0.3 numerical aperture EUV microfield optic," J. Vac. Sci. & Technol. B **23**, 2003-2006 (2005).
23. P. Naulleau, K. Goldberg, E. Anderson, K. Dean, P. Denham, J. Cain, B. Hoef, K. Jackson, "Characterization of the synchrotron-based 0.3 numerical aperture extreme ultraviolet microexposure tool at the Advanced Light Source," J. Vac. Sci. & Technol. B **23**, 2840-2843 (2005).
24. C. Ahn, H. Kim, K. Baik, "A novel approximate model for resist process," Proc. SPIE **3334**, 752-763 (1998).
25. P. Naulleau, "Verification of point-spread function based modeling of an EUV photoresist," Appl. Opt. **43**, 788-792 (2004).
26. G. Gallatin, "Resist Blur and Line Edge Roughness," Proc. SPIE **5753**, 38-52 (2005).
27. A. Ma, J. Park, K. Dean, S. Wurm, and P, Naulleau, "Benchmarking Commercial EUVL Resists at SEMATECH," *these proceedings*.